

# An Interface-Enriched eXtended Finite Element-Level Set Simulation of Solutal Melting of Additive Powder Particles during Transient Liquid Phase Bonding

A. GHONEIM, J. HUNEDY, and O.A. OJO

A new numerical simulation model is developed by using an interface-enriched eXtended Finite Element-Level Set (XFE-LS) method to study the solute-induced melting of additive powder particles (APPs) during transient liquid phase (TLP) bonding. The robust model captures rapidly occurring concurrent interfacial events at multiple propagating liquid-solid interfaces to simulate the melting behavior. In contrast to the critical assumption in analytical models, numerical calculations show that solute-transport into the APPs during the equilibration of the liquid composition is a significant factor that affects the APPs melting behavior. Also, the study shows that the solute-transport dependence of extent of APPs melting is influenced by the kinetics of solid-state solute diffusion within the particles. The understanding generated by the numerical analysis has resulted in the use of interlayer powder mixture that contains base-alloy APPs to produce single crystal TLP joint that has matching crystallographic orientations with single crystal substrate material, at a substantially reduced processing time, which has been previously considered unfeasible.

DOI: 10.1007/s11661-012-1412-1

© The Minerals, Metals & Materials Society and ASM International 2012

## I. INTRODUCTION

ADVANCED alloy design and improved solidification processing techniques have resulted in the development of single crystal (SC) precipitation strengthened nickel (Ni)-base superalloys with remarkable elevated temperature properties for producing a new generation of aero-engine components required for higher engine efficiency and lower greenhouse emissions. However, the development that has occurred with SC aerospace superalloys in the past two decades has not been matched by adequate understanding of appropriate techniques for joining these materials without deleterious stray-grains formation. Joining is not only essential for the economical manufacturing of complex shaped engine components, but also vital for the repair and refurbishment of service-degraded aero-engine parts. SC precipitation strengthened Ni-base superalloys are extremely difficult to join by conventional fusion welding processes due to their high susceptibility to cracking during welding and post-weld thermal treatments.<sup>[1,2]</sup> Transient liquid phase (TLP) bonding, also known as diffusion brazing, has evolved as an attractive alternate technique for joining the difficult-to-weld SC superalloys and other structural alloys.<sup>[1–5]</sup>

In TLP bonding, an interlayer material that contains melting-point depressing (MPD) solute and sandwiched

between two substrates melts at the bonding temperature and rapidly attains equilibrium through liquid-phase dissolution of the base-material into the molten interlayer alloy. This is succeeded by isothermal solidification of the liquated insert by solid-state diffusion of the MPD solute away from the liquid into the solid substrates. An approach that has been found effective for reducing the liquid-phase dissolution of the base-material, which is also known as liquid-metal erosion, during TLP bonding, involves the use of a powder mixture as the interlayer material. The powder mixture consists of regular TLP bonding filler alloy powder that contains the MPD solute and an additive powder alloy that is essentially free of the MPD solute, usually the base-alloy powder. Aside from reduction of substrate liquid-phase erosion, the use of the powder mixture as the interlayer material enables the desirable enrichment of the TLP joint region with the base-material alloying element for enhanced joint properties.

Unfortunately, the beneficial powder mixture has been generally considered unsuitable for joining SC superalloys, due to the formation of stray-grains within the joint region, which compromises the properties of bonded SC materials. The stray-grains are formed when additive powder particles (APPs) are partially melted by the liquated filler alloy in the interlayer powder mixture during bonding. Solute-induced melting, henceforth referred to as “melting”, has been previously studied.<sup>[6–8]</sup> However, the understanding of the behavior of APPs melting during TLP bonding by the molten filler alloy which controls the formation of deleterious stray-grain formation is limited for several cogent reasons. The melting process involves rapidly occurring concurrent interfacial events at multiple liquid-solid interfaces

---

A. GHONEIM, Research Associate, J. HUNEDY, Graduate Student, and O.A. OJO, Associate Professor, are with the Department of Mechanical and Manufacturing Engineering, University of Manitoba, Winnipeg, MB R3T 5V6, Canada. Contact e-mail: olanrewaju.ojo@ad.umanitoba.ca

Manuscript submitted March 24, 2012.

Article published online October 17, 2012

of the APPs, in the order of a few seconds, which are significantly influenced by interdependent material and process variables. An appropriate theoretical model, rather than an exclusive experimental approach, is crucial for a proper study of the melting process. This is required for studying rapid evolution of the APPs during melting, by concurrently monitoring the displacements and migration rates of the propagating multiple liquid-solid interfaces and how they change with time and location with respect to adjacent powder particles. Analytical TLP bonding models are unsuitable for performing this type of analysis, and this is further compounded by the fact that the diffusion of the MPD solute into APPs is generally ignored in these models due to difficulty in modeling simultaneous solute diffusion in APPs and their melting by the surrounding liquid phase.<sup>[9]</sup> Rather, a numerical modeling approach is best suited for the analysis.

However, most of the available TLP bonding numerical models rely on simplistic 1-D analysis by using conventional interface-tracking methods to model the moving interphase boundary and the bonding process.<sup>[10–12]</sup> In these models, the interface is often assumed to be perfectly planar, and symmetry is assumed at the joint. These models are unsuitable for simulating APP melting since the process involves non-symmetrical distribution of powder particles, and solute diffusion across their curved undulating liquid-solid interfaces during melting departs from simplified 1-D approximation. In spatial dimensions higher than 1-D, the solutions of moving boundary problems for complex geometries and interfacial kinetics by using conventional interface-tracking methods is often cumbersome. The method involves the introduction of nodal points at the propagating interphase boundary, and the transport equations are solved by using moving-mesh techniques to ensure conformance of the mesh with the migrating interface. A re-meshing step is often required as the interface propagates to ensure high quality elements and avoid severe mesh distortion. This re-meshing step is often computationally expensive especially as the number of interfaces increase and as the geometry increases in complexity. Furthermore, as the interface propagates, nodal points at the interface can get too close together or too far apart, which can render the analysis significantly inaccurate. Major numerical difficulties are also encountered when the splitting of propagating interphase interfaces occurs, such as during melting of APPs. To ensure the accuracy of the solutions an extra step is often required where nodal points are explicitly added at the interface if interfacial nodes get too far apart, or removed if they get too close, which would require further mesh adjustment and adaptation for every time step as the interface propagates. This rather explicit treatment significantly complicates the algorithm and decreases the efficiency of computations. Due to these aforementioned difficulties, conventional interface-tracking methods are often limited to simple geometries and interfacial topologies.

To mitigate the limitations of existing TLP bonding numerical models and avoid the limitations of conventional interface-tracking methods, a new numerical

model is developed in this work by using an interface-enriched eXtended Finite Element-Level Set (XFE-LS) method to study and enable a better understanding of the melting behavior of arbitrarily shaped and randomly distributed APPs during TLP bonding. The interface-enriched eXtended Finite Element Method (XFEM) is implemented to enable robust handling of the discontinuities at the liquid-solid interfaces while the Level Set Method (LSM) is used to accurately simulate the evolution of the propagating liquid-solid interfaces. The new approach eliminates the requirement of aligning the computational mesh with the rapidly evolving liquid-solid interfaces, and hence, eliminates the re-meshing that is typically required in conventional finite element methods to avoid mesh distortion near propagating interphase boundaries. The development of this novel model, its implementation, simulation results and experimental verification, with respect to the melting behavior of APPs during TLP bonding, are discussed in this paper.

## II. MATHEMATICAL FORMULATION AND IMPLEMENTATION

### A. Finite Element Description of the TLP Bonding Problem

Consider a domain  $\Omega$  that consists of a solid phase  $\Omega_S$  and a liquid phase  $\Omega_L$  such that  $\Omega = \Omega_S \cup \Omega_L$  and  $\Omega_S \cap \Omega_L = 0$  (Figure 1). To describe the particle-liquid interface  $\Gamma(t)$  at time  $t$ , we introduce a field  $\Phi$  such that the interface is the zero level set of  $\Phi$ :

$$\Gamma(t) = \{\mathbf{x} \in \Omega : \Phi(\mathbf{x}, t) = 0\}$$

where the field  $\Phi$  is taken as a signed distance function such that the distance of point  $\mathbf{x}$  to the transition interface at time  $t$  can be represented as:

$$d(\mathbf{x}, t) = \pm \min\|\mathbf{x} - \mathbf{x}_\Gamma\|$$

where  $\mathbf{x}_\Gamma$  lies on  $\Gamma(t)$ . The level set function  $\Phi$  can then be defined as the signed distance function from the interface:

$$\Phi(\mathbf{x}, t) = \pm \min\|\mathbf{x} - \mathbf{x}_\Gamma\| = \begin{cases} d(\mathbf{x}, t) & \mathbf{x} \in \Omega_L \\ 0 & \mathbf{x} \in \Gamma \\ -d(\mathbf{x}, t) & \mathbf{x} \in \Omega_S \end{cases}$$

The diffusion of the MPD solute can be described by using Fick's second law of diffusion:

$$\frac{\partial C_p}{\partial t} = \nabla(D_p \nabla C_p) \quad [1]$$

where  $C_p$  is the composition of the liquid solid phases,  $D_p$  is the interdiffusion coefficient,  $t$  is time and subscript  $p = S$  for solid and  $p = L$  for liquid.

Due to the diffusion of the MPD solute, the liquid-solid interface must migrate to ensure mass balance. Migration of the interface can be expressed by using Eq. [2], which is analogous to the Stefan equation for thermally induced phase transformation.

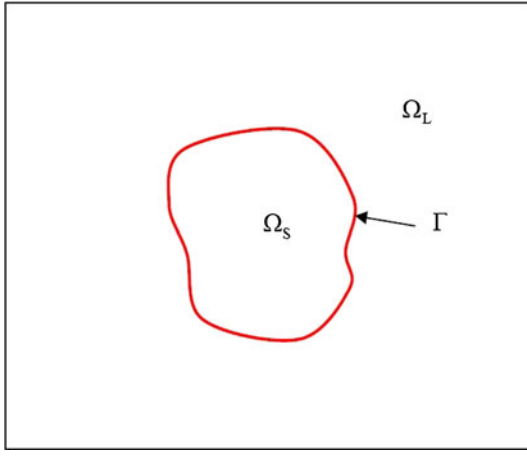


Fig. 1—Illustration showing the liquid  $\Omega_L$ , solid  $\Omega_S$  and interface  $\Gamma$ .

$$(C_L^0 - C_S^0)\mathbf{V}_n = -D_L \frac{\partial C_L}{\partial \mathbf{n}} + D_S \frac{\partial C_S}{\partial \mathbf{n}} \quad [2]$$

where  $\mathbf{V}_n$  is the velocity of the interface in a direction normal to the interface,  $C_L^0$  is the liquidus concentration,  $C_S^0$  is the solidus concentration at the bonding temperature and  $(\partial/\partial \mathbf{n})$  is the directional normal to the interface.

The conditions at the interface  $\Gamma(t)$  include two Dirichlet-type boundary conditions for each side of the interface such that:

$$C(\Gamma, t) = C_S^0 \quad \text{for } \mathbf{x} \in \Omega_S$$

and

$$C(\Gamma, t) = C_L^0 \quad \text{for } \mathbf{x} \in \Omega_L$$

By using the Galerkin finite element method, the introduction of interpolation functions  $N_i(x, y)$  over an area  $A$  and the denoting of the phase with subscript  $p$  such that  $p = L$  in liquid and  $p = S$  in solid, Eq. [1] can be expressed as:

$$\iint_A N_i(x, y) \left\{ \frac{\partial}{\partial x} \left( D_p^x \frac{\partial C}{\partial x} \right) + \frac{\partial}{\partial y} \left( D_p^y \frac{\partial C}{\partial y} \right) - \frac{\partial C}{\partial t} \right\} dA = 0 \quad [3]$$

By assuming that diffusivity is independent of the concentration, the above equation can be re-expressed as:

$$\begin{aligned} & \iint_A \left( D_p^x \frac{\partial C}{\partial x} \frac{\partial N_i}{\partial x} + D_p^y \frac{\partial C}{\partial y} \frac{\partial N_i}{\partial y} \right) dA + \iint_A \left( N_i \frac{\partial C}{\partial t} \right) dA \\ & = - \oint_S (J_x + J_y) N_i dS \end{aligned} \quad [4]$$

where  $J_x$  and  $J_y$  represent the flux of diffusing solute in the  $x$  and  $y$  dimensions, respectively. The above equation can be expressed in a matrix form as follows:

$$\begin{aligned} & \iint_A \left( D_p^x \left[ \frac{\partial N}{\partial x} \right]^T \left[ \frac{\partial N}{\partial x} \right] + D_p^y \left[ \frac{\partial N}{\partial y} \right]^T \left[ \frac{\partial N}{\partial y} \right] \right) \{C_p\} dA \\ & + \iint_A [N]^T [N] \{ \dot{C}_p \} dA = - \oint_S J_s [N]^T dS \end{aligned} \quad [5]$$

where symbol  $[ ]^T$  is the transpose matrix and  $\{ \dot{C} \}$  is the partial differential for the nodal concentrations with respect to time. The diffusion equations in the liquid and solid phases, Equation [5], can be expressed in a global matrix form:

$$[K]\{C\} + [M]\{\dot{C}\} = \{F\} \quad [6]$$

The  $[K]$  term is the global stiffness matrix,  $[M]$  is the global mass matrix and  $\{F\}$  is the global force matrix. The use of an implicit scheme to solve this equation yields the following equation expressed in a matrix form:

$$\{C\}^{j+1} = (\Delta t[K] + [M])^{-1} (\Delta t\{F\} + [M]\{C\}^j) \quad [7]$$

where  $\Delta t$  is the time step,  $j$  is the current time and  $j + 1$  is the future time.

## B. Interface-Enriched Extended Finite Element Formulation

In conventional finite element methods, modeling of moving boundaries, such as moving interphase interfaces, often involve moving-mesh or adaptive meshing techniques to maintain alignment of the interfacial elements with the moving interface. Constant re-meshing is required to avoid severe mesh distortion due to the moving interface, which is rather cumbersome and computationally expensive especially in 3D analysis. Failure to re-mesh can severely affect the accuracy of the finite element solution. Additionally, difficulties arise whenever merging and splitting of the interfaces occur.

An alternative and more recent approach in finite element analysis involves Eulerian methods in which calculations are carried out on a non-conforming fixed mesh where the interfaces can be embedded into the elements rather than aligned (Figure 2). A relatively new approach for representing localized behavior in finite elements is termed the partition of unity method (PUM) proposed by Melenk and Babuska<sup>[13]</sup> where classical approximation is extended by augmenting a set of nodal shape functions with the production of a subset of these same shape functions and local enrichment functions. The XFEM is a variation of this framework, which alleviates the shortcomings associated with conventional finite element methods in dealing with the discontinuities present in moving boundary problems. This is accomplished by locally extending the basis (or shape) functions used to reproduce the desired local feature, such as discontinuity.

In the XFEM framework, for a domain  $\Omega$  with arbitrarily distributed interfaces on a structured mesh as shown in Figure 2, the standard FEM is modified by

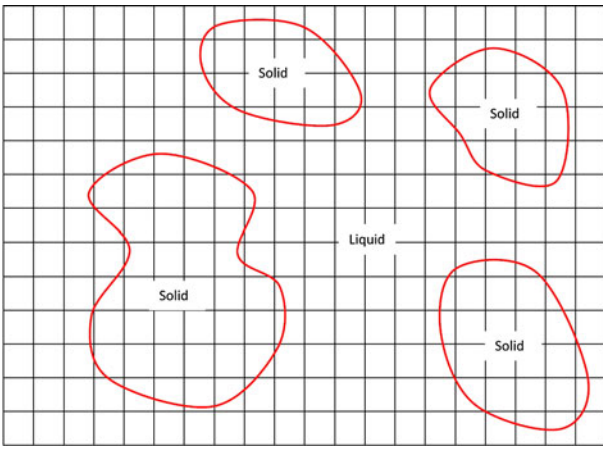


Fig. 2—Arbitrarily distributed interfaces embedded in the structured elements in the XFEM.

locally extending the basis functions and approximating the solution as follows<sup>[14]</sup>:

$$C(\mathbf{x}) = \sum_{i=1}^{n_{std}} N_i(\mathbf{x})C_i + \sum_{j=1}^{n_{enr}} \psi_j(\mathbf{x})a_j \quad [8]$$

where  $N_i(\mathbf{x})$  are the standard finite element shape functions for node  $i$ ,  $C_i$  are the nodal degrees of freedom,  $\psi_j(\mathbf{x})$  are the enrichment functions and  $a_j$  are the nodal enrichment degrees of freedom.  $n_{std}$  and  $n_{enr}$  are the number of nodal standard degrees of freedom and nodal enriched degrees of freedom, respectively.

The enriched elements are defined as elements that are cut by the interface as determined by the values of the level set function. A node is enriched if at least one of its surrounding elements is intersected by the interface (Figure 3). As the interface evolves with time, the set of enriched elements and nodes is also changing with time. The enrichment functions  $\psi_j$  are required to be linearly independent of each other and also independent of standard finite element basis functions. In classical XFEM, nodes are enriched for elements intersected by the interface<sup>[15]</sup>; thus, there will be elements in which some of the shared nodes will be enriched while others are not. These are referred to as “blending elements” and it is obvious that the shape functions for such elements will no longer satisfy the partition of unity requirement:

$$\sum N_i(\mathbf{x}) = 1$$

It has been shown<sup>[15–18]</sup> that these blending elements can result in degrading the convergence of the solution for certain enrichment functions, and certain techniques are therefore required to overcome these difficulties.

Many problems in phase transformation, including TLP bonding, require imposing the essential boundary conditions (EBC) directly at the interfaces, which is rather difficult in the XFEM. Exact and direct imposition of the EBC at the interfaces is most desirable in sharp-interface phase transformation problems as it directly influences the gradients on each side of the interface and hence directly influences the extent of its migration.

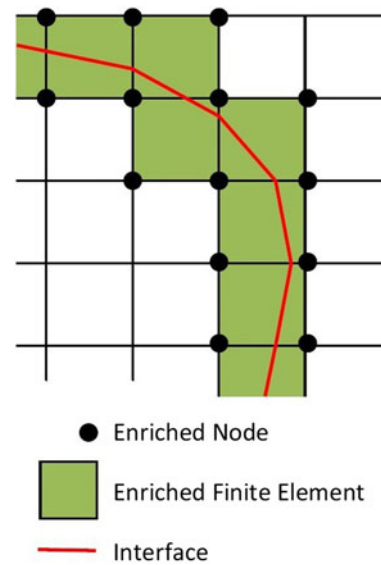


Fig. 3—Nodal enrichment in the classical XFEM.

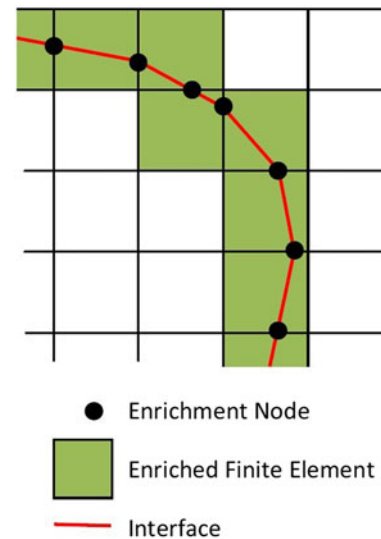


Fig. 4—Interface enrichment for elements intersected by the interface in the interface-enriched XFEM.

Generally, in conventional moving-mesh finite element models, the interfacial nodes always coincide with the edges of adjacent elements and imposing Dirichlet boundary conditions is often simple and straightforward. However, in XFEM, the interface is embedded into the element and no longer aligned with the element edges. Imposing the essential boundary conditions requires them to be enforced where they can be resolved by methods such as the penalty method or Lagrangian multipliers. Penalty methods impose the EBC only approximately and some studies have shown that penalty methods are sensitive to numerical parameters and can potentially result in ill conditioned global matrices with mesh refinement.<sup>[19]</sup> Lagrange multipliers techniques are computationally expensive as they destroy the positive definiteness and bandedness of the resulting algebraic

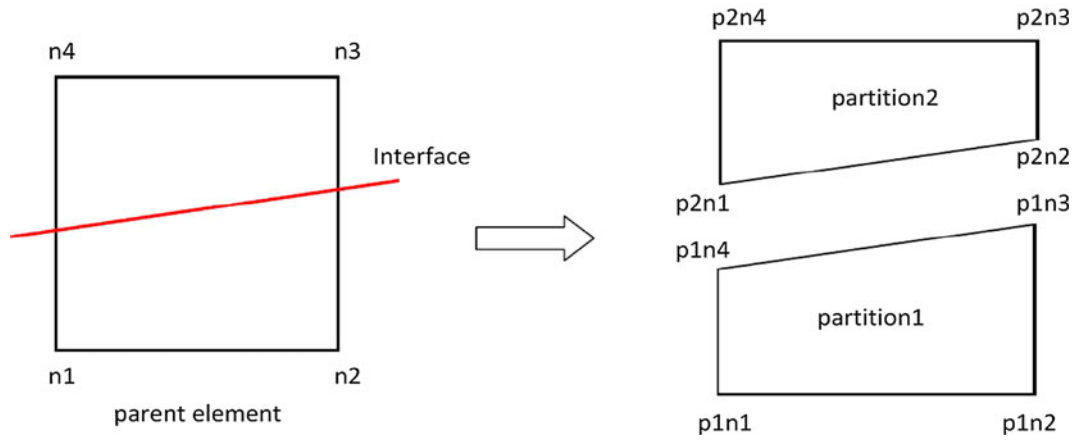


Fig. 5—Partitioning of an element intersected by an interface for interfacial enrichment.

equations system and have been reported to be susceptible to stability problems and can lead to over-constrained problems if the choice of the finite element subspace for the Lagrange multiplier field does not satisfy the inf-sup condition.<sup>[20]</sup> Numerical oscillations may occur as a result of imposing Dirichlet boundary conditions by using Lagrange multipliers, especially in elements in which the interface is close to the finite element nodes.<sup>[21]</sup>

To overcome these obstacles in the present work, interfacial enrichment is used instead of nodal enrichment for elements intersected by the interface (Figure 4). For an element intersected by the interface, a unified enrichment is achieved by sharing the same degrees of freedom between interface nodes and adjacent elements, and not nodes of the original mesh. Consider a rectangular element intersected by the interface as shown in Figure 5. Enriching of the solution field  $C(\mathbf{x})$  at the intersection nodes between the interface and the element can be expressed as:

$$C(\mathbf{x}) = N_1^{\text{parent}} C_1 + N_2^{\text{parent}} C_2 + N_3^{\text{parent}} C_3 + N_4^{\text{parent}} C_4 + \left( N_4^{\text{partition1}} + N_1^{\text{partition2}} \right) a_1 + \left( N_3^{\text{partition1}} + N_2^{\text{partition2}} \right) a_2 \quad [9]$$

which can be expressed as:

$$C(\mathbf{x}) = N_1^{\text{parent}} C_1 + N_2^{\text{parent}} C_2 + N_3^{\text{parent}} C_3 + N_4^{\text{parent}} C_4 + \psi_1 a_1 + \psi_2 a_2 \quad [10]$$

where

$$\psi_1 = N_4^{\text{partition1}} + N_1^{\text{partition2}} \quad \text{and} \quad \psi_2 = N_3^{\text{partition1}} + N_2^{\text{partition2}} \quad [11]$$

This can then be extended into:

$$C(\mathbf{x}) = \sum_{i=1}^{n_{\text{std}}} N_i(\mathbf{x}) C_i + \sum_{j=1}^{n_{\text{enr}}} \psi_j(\mathbf{x}) a_j$$

which is the same equation as that of the standard XFEM Eq. [8]. However in contrast to the classical XFEM, the system of equations is “extended” by

imposing the additional degrees of freedom directly at the interface instead of at the intersected element nodes. This approach allows for a smaller system of equations to be solved than in the classical XFEM and ensures that there will always be nodes directly associated with the interface, so imposing the essential boundary conditions at the interface can be done exactly and easily. To evaluate the enrichment functions, elements intersected with the interface are partitioned into the minimum number of integration elements required to ensure accurate quadrature. The enrichment function which corresponds to an interfacial node is constructed as the linear combination of the Lagrangian shape functions in the integration elements with a unity value at that node. In the present work, for cases where an interfacial node is too close to a node in the parent element, scaling of the enrichment functions is employed to avoid ill-conditioned global matrices as discussed in Reference 22 and 23.

A standard procedure in finite element analysis is numerical integration over the elements by using Gaussian quadrature. Every element in a mesh is associated with a material property used to calculate the integral. However, in XFEM, the interface cuts the element, and as a result, part of the element is associated with one phase while the other is associated with another phase, each of which has its own properties. By using a standard Gaussian quadrature over the whole element, this will affect the accuracy of the calculated results since not all of the integration points lie on the same phase. As a result, in XFEM, the elements intersected by the interface are partitioned to enable accurate numerical integration. In the literature, this partitioning is often done by using sub-triangles or sub-rectangles.<sup>[15]</sup> In the present work, the elements intersected by the interface are partitioned with sub-triangles as illustrated in Figure 6. More information about the partitioning of the elements in XFEM can be found in Reference 24.

### C. Level Set Method Formulation

The LSM was first developed by Sethian and Osher<sup>[25]</sup> as a means to capture the evolution of propagating fronts. In the LSM, the interface is implicitly represented by the

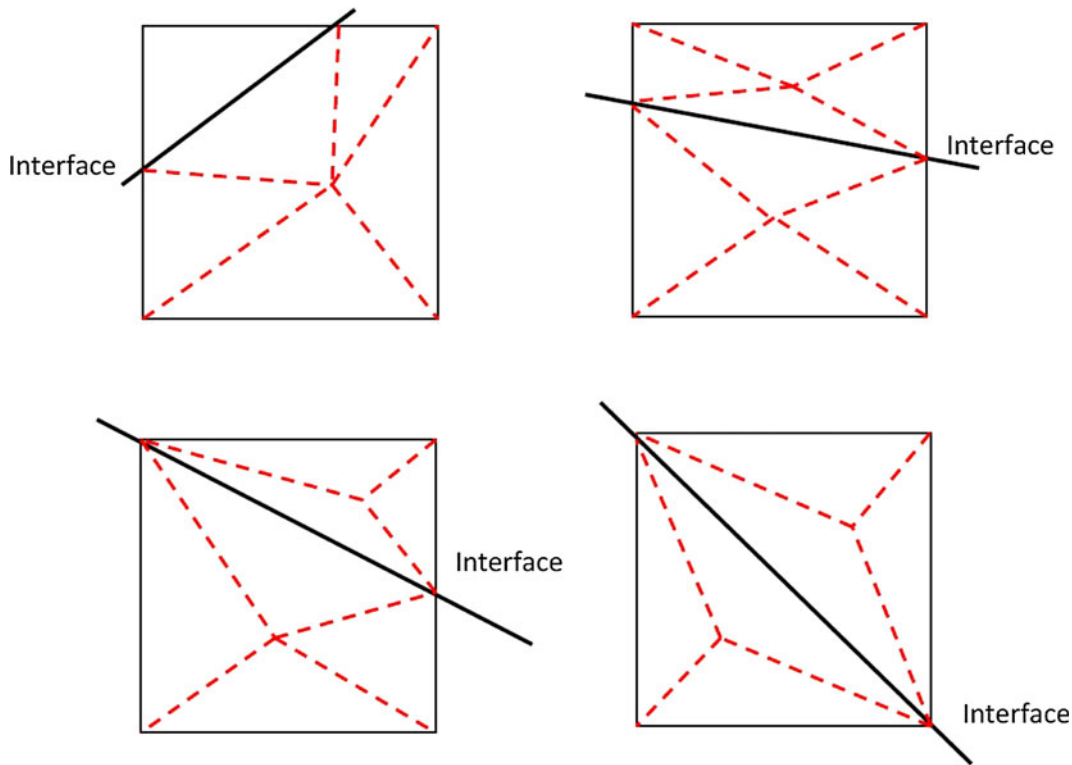


Fig. 6—Partitioning of elements intersected by the interface for numerical integration calculations.

zero of an iso-surface function  $\Phi$ , the so called level set function. A level set value obtained from a signed distance function at a node on a computational grid represents the minimum distance between that node and the interface. It exhibits a negative value at one phase while it is positive at another. This implicit representation of an interface by using a level set function has a number of very important advantages. At any given time, the location of the interface can be extracted by obtaining the zero iso-contour of the level set function. Useful information of the relative distance between the grid nodes and the interface are readily available from the nodal values of the level set function. Distinction between the phases present in the domain is easily extracted from the sign of the level set function value at each node. Important information that can be extracted from the level set function includes calculating the normal, which is expressed as:

$$n = \frac{\nabla\Phi}{\|\nabla\Phi\|} \quad [12]$$

and the local curvature, which is expressed as:

$$\kappa = \nabla \cdot \frac{\nabla\Phi}{\|\nabla\Phi\|} = \frac{\Phi_{xx}\Phi_y^2 - 2\Phi_y\Phi_x\Phi_{xy} + \Phi_{yy}\Phi_x^2}{(\Phi_x^2 + \Phi_y^2)^{3/2}} \quad [13]$$

When the speed  $V_n$  of the interface in the direction normal to the interface is known, the interface evolution can be mapped into an evolution of the level set function with Hamilton-Jacobi equations. Evolution of the level set function is represented by:

$$\frac{\partial\Phi}{\partial t} + V_n\|\nabla\Phi\| = 0 \quad [14]$$

To solve the level set evolution equation, upwind difference schemes and schemes borrowed from the solution of hyperbolic conservation laws are generally used. One drawback of the level set approach is the requirement that the speed function  $V_n$  be given in the entire domain of  $\Phi$ . In the present work, to calculate the extended velocity on the entire domain  $V_n^{\text{ext}}$ , the level set equation is re-written as:

$$\frac{\partial\Phi}{\partial t} + V_n^{\text{ext}}\|\nabla\Phi\| = 0 \quad [15]$$

where  $V_n^{\text{ext}}$  is some velocity field that agrees with the speed function  $V_n$  on a zero level set.

$$V_n^{\text{ext}}|_{\Phi=0} = V_n \quad [16]$$

A fast marching method is used to calculate  $V_n^{\text{ext}}$  as described in Reference 26. The following equation is solved:

$$\|\nabla\Phi\| = \frac{1}{F(x)} \quad [17]$$

and the front is then systematically advanced by marching outwards from the boundary in an upwind fashion.  $V_n^{\text{ext}}$  is constructed by computing the signed distance function  $\Phi$  obtained by letting  $F(x) = 1$  while simultaneously solving the associated equation:

$$\mathbf{V}_n^{\text{ext}} \cdot \nabla \Phi = 0 \quad [18]$$

Conventional differencing schemes will fail to evolve  $\Phi$ , therefore, a higher order differencing scheme is often required. In the present work, a Weighted Essentially Non-Oscillating (WENO) difference scheme is used as discussed in Reference 26. Time integration is carried out with the Euler forward method in which stability is enforced by using the Courant-Friedrichs-Lewy (CFL) condition.<sup>[26]</sup> After  $\Phi$  is evolved, it generally does not remain a signed distance function. This may lead to flat/steep gradients of  $\Phi$  near the interface, which result in inaccurate approximation of the front velocity. In order to prevent these effects, re-initialization of the level set function to a distance function is often required. This is done by using the following equation<sup>[26]</sup>:

$$\frac{\partial \Phi}{\partial \tau} = \text{sign}(\Phi)(1 - \|\Phi\|) \quad [19]$$

where  $\tau$  is the virtual time not related to the actual computation time. The  $\text{sign}(\Phi)$  is calculated by using:

$$\text{sign}\Phi = \frac{\Phi}{\sqrt{\Phi^2 + \|\nabla\Phi\|^2 \Delta^2}} \quad [20]$$

where  $\Delta$  is the grid size.

#### D. Model Assumptions and Implementation

The current numerical simulation model describes diffusion-controlled isothermal phase changes under the following assumptions:

1. There is local equilibrium at the liquid-solid interface.
2. Atomic diffusion can be described by Fick's second law of diffusion.
3. The molar volume is assumed constant irrespective of phase or concentration.
4. Diffusivity of the MPD solute is independent of concentration in each phase.
5. Grain boundaries are assumed absent, which is valid for single crystal materials.

A computational code which implements the coupled XFE-LS model for simulation of melting of APP in Ni-based materials was developed and written by using Object-Oriented Programming (OOP) techniques. The pre-processor allocates the required memory and initializes the variables as per user defined parameters. The XFEM solver calculates the MPD solute distribution in the liquid and solid phases which are used by the LSM solver to calculate the interfacial speed and the transient evolution of the level set function. A fixed grid is created and the location of powder particles is initialized along with initializing the signed distance function. At each time step, the following algorithm is implemented:

1. Calculate the future MPD solute distribution in the whole domain by using the XFEM solver. From the level set function, elements intersected by the

interface are partitioned and enriched. Elements away from the interface are solved by using the conventional finite element method.

2. Calculate the local speed at the interface.
3. Extend the interfacial velocity to a sufficient number of nodes away from the interface by using the fast marching method.
4. By using the extended interfacial velocity calculated in (3), calculate the future level set function by using the high-order difference WENO scheme.
5. Reinitialize the level set function calculated in (4) for virtual time steps that are user specified to force the level set function to be a signed distance function.

Steps 1 to 5 are then repeated for the next time step. The MPD solute distribution is calculated in the whole domain for all phases in a single step. The use of the level set function governs the final interfacial evolution required for XFEM processing. It is clear from the algorithm that no explicit tracking or treatment of the interfaces is necessary. The final location of the interface is extracted by calculating the zero iso-contour of the level set function as part of the post-processing stage.

To calculate the time required to achieve complete isothermal solidification of the interlayer liquid after the complete melting of the powder particles, the new XFE-LS model is coupled with the Moving-Mesh Finite Element (MMFE) model previously developed by the present authors.<sup>[27]</sup> The MMFE model developed by Ghoneim *et al.*<sup>[27]</sup> has been also used to study an aspect of asymmetric diffusional solidification during TLP bonding of dissimilar superalloys.<sup>[28]</sup> Since the melting of the powder particles generally occurs much faster than the isothermal solidification stage, both are in conflict with one another for direct numerical analysis. The capturing of intricate interfacial dynamics during the melting stage requires much smaller time stepping and much finer meshes. In contrast, however, efficient calculation of the solidification of the interlayer liquid requires larger time stepping and considerably coarser meshes at the solid base materials. Therefore, in the present work, a coupling scheme is used to ensure efficient and accurate calculation of the interfacial dynamics during both stages. Calculations of the melting of arbitrarily shaped and randomly distributed powder particles are done by using the new XFE-LS model which uses a fine computational grid. Upon complete melting of the powder, the results obtained by the XFE-LS model are fed into the MMFE model to calculate the rate of isothermal solidification and the final solidification time. The MMFE was derived by using a fully implicit solute-conserving scheme which enables much larger time steps while maintaining the stability of the solution.<sup>[24]</sup>

### III. RESULTS AND DISCUSSION

#### A. Modeling Asymmetric Solute Concentration Gradients and Interfacial Splitting

In the present work, the binary Ni-B system is considered for numerical analysis where boron is the MPD solute. Relevant data of the Ni-B phase diagram

**Table I. Ni-B Phase Diagram Data Used in Simulations**

Parameter	Value
System	Ni-B
Eutectic concentration	17 at. pct (3.6 wt pct)
Eutectic temperature [K (°C)]	1366 (1093)
Bonding temperature [K (°C)]	1373 to 1523 (1100 to 1250)
Initial boron concentration in APPs	0 at. pct (0 wt pct)
Initial boron concentration in liquated filler alloy	17 at. pct (3.6 wt pct)
Diffusion of boron in liquid	$5E-10$ m <sup>2</sup> /s
Activation energy for diffusion in solid	226 kJ/mol
Solid diffusion frequency factor	$0.14$ m <sup>2</sup> /s

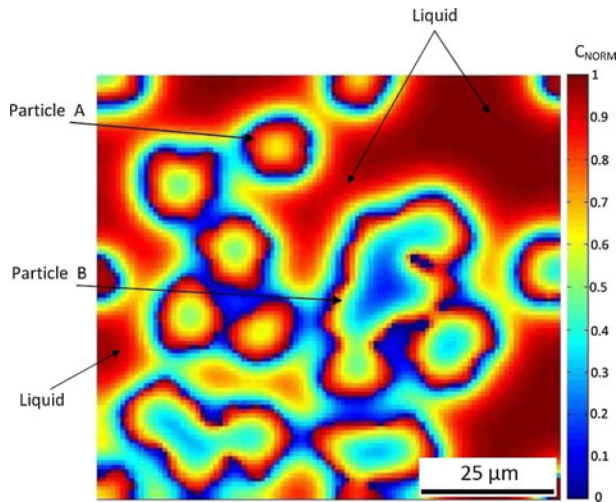


Fig. 7—Normalized MPD solute (boron) distribution in liquid and powder particles. The legend shows normalized concentrations of the MPD solute in the liquid phase and solid particles.

used in this work are listed in Table I.<sup>[29]</sup> Preliminary verification of the newly developed model showed that it is able to concurrently capture the intricate and rapidly occurring interfacial events at multiple liquid-solid interfaces on APPs during melting, including cases that are problematic with the use of conventional interface-tracking methods. Figure 7 shows a non-symmetrical case that involves randomly distributed APPs of varying sizes and shapes, and thus, differing melting behaviors. As particle “A” is nearly saturated with the MPD solute, a larger particle “B” is still able to assimilate more solute, thus, setting up an asymmetric interfacial solute concentration gradient, which is crucial in the melting process. In addition, Figure 8 shows the splitting of the liquid-solid interface of a single powder particle into two separate liquid-solid interfaces due to the disintegration of the particle into separate particles during melting. This scenario is a typical example of cases that are generally problematic to be modeled by the conventional interface-tracking method, and caused by the non-planar morphology of the liquid-particle interface and concomitant uneven migration velocity along the curved interphase boundary, which are readily captured by the new model.

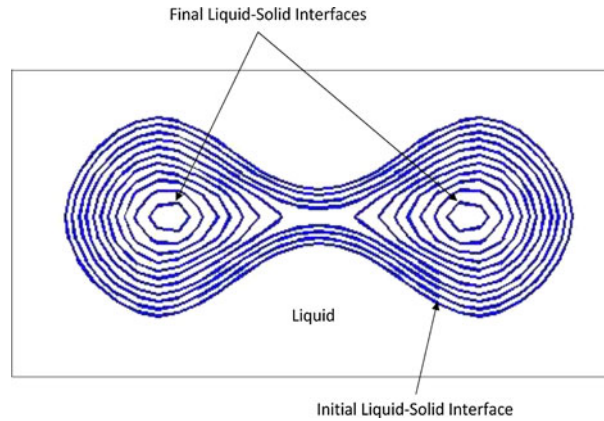


Fig. 8—Numerical simulation of interfacial splitting during melting of an APP.

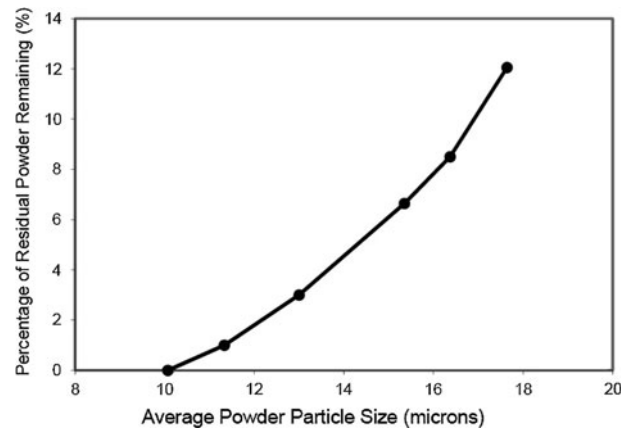


Fig. 9—Numerical simulation of the effect of powder particle size on residual powder remaining in liquid after simulation 500 time steps.

### B. Influence of Solute-Transport in APPs on Their Melting

According to the classical theory of TLP bonding, the main thrust for the melting of APPs into the surrounding molten filler alloy, at the initial stage of the bonding process, is to reduce the concentration of the MPD solute in the liquid to the equilibrium liquidus value at the bonding temperature. It has been noted that in analytical TLP bonding models, this equilibration process is assumed to exclusively involve the addition of solvent element from the solid powder particles to the surrounding liquid without concomitant transfer of the MPD solute from the liquid into the particles by solid-state diffusion within the particles.<sup>[30]</sup> This is due to the difficulty in modeling simultaneous solid-state solute-transport within APPs and their solute-induced melting by the surrounding liquid. The robust numerical model developed in this work, which does not have this major limitation, shows that the solute-transport plays a significant role in the equilibration process and that the extent of APP melting is dependent on the diffusion rate of the solute within the powder particles. The faster the solute-transport rate, as controlled by solid-state



**Table II. Materials Nominal Composition (Weight Percent)**

Material	Ni	Cr	Co	Mo	W	Nb	Al	Ti	Fe	Ta	C	B	Zr	S
IN738	bal.	15.84	8.5	1.88	2.48	0.92	3.46	3.47	0.07	1.69	0.11	0.012	0.04	0.001
Nicrobraz 150	bal.	15	—	—	—	—	—	—	—	—	0.03	3.5	—	—

diffusion, the lesser the extent of the APPs melting. According to Fick's second law of diffusion, the kinetics of solute-transport by solid-state diffusion is controlled by the extent of change in solute concentration gradient per unit distance  $[\frac{\partial}{\partial x}(\frac{\partial C}{\partial x})]$  away from the liquid-solid interface within the APPs. Accordingly, a major factor that influences the extent of APPs melting is  $\frac{\partial}{\partial x}(\frac{\partial C}{\partial x})$  inside the powder particles.

Figure 9 shows the numerical simulation results of variation of APP melting with initial APP size for a fixed ratio of 50 pct, as the particle size can be varied to achieve the same ratio of filler alloy powder particles to APPs,  $R_{FA}$ . The variation in the extent of APP melting APP dissolution with particle size, for a constant value of  $R_{FA}$ , indicates that the size of the powder particles influences the extent of melting of the powder particles. In order to verify the validity of the numerical simulation result, experiment was performed with the use of an interlayer powder mixture that contained IN 738 super-alloy as the APPs and Nicrobraz 150 as the filler alloy powder where boron is the MPD solute. IN 738 was used as the substrate material. The chemical compositions of the alloys are listed in Table II. Two types of powder mixtures were used; Type 1 consisted of fine APPs with an average 25  $\mu\text{m}$  and Type 2 consisted of coarse APPs with an average size of 85  $\mu\text{m}$ . The extent of the melting of the APPs in Types 1 and 2 powder mixtures with a fixed  $R_{FA}$  value of 7:3, was examined after a holding time of 4 hours, which is more than the time required to achieve equilibration. Figures 10 and 11 show the micrographs of the resultant Types 1 and 2 powder mixtures, respectively, after holding for 4 hours at 1373 K (1100 °C). In contrast to the Type 2 mixture, the microstructure of the Type 1 mixture is free of residual APPs, but instead consists of a solidification dendritic microstructure. There are three main phases that form by on-cooling non-equilibrium solidification of residual interlayer liquid produced by the filler alloy and base-alloy materials used in this work. The phases are nickel-base boride, chromium-base boride and nickel-base austenitic solid-solution phase.<sup>[31]</sup> The present results show that while the coarse APPs in the Type 2 mixture remained incompletely melted, a reduction in the powder size in the Type 1 mixture with the same  $R_{FA}$  resulted in the complete melting of the APPs. The experimental results validate the numerical analysis that indicates that the extent of the APPs melting is dependent on the amount of solute-transport, as controlled by the rate of the solute-transport, rather than through the total surface area available for solute-transport by solid-state diffusion. This finding, which has not been previously reported and cannot be achieved by current analytical models, is fundamentally vital to the proper understanding of the conditions that enable stray-grains formation during TLP bonding of

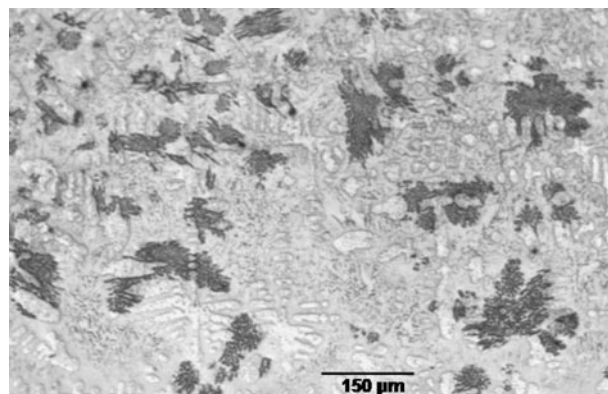


Fig. 10—Microstructure of Type 1 powder mixture with completely melted of fine APPs with  $R_{FA}$  of 7:3 at 1373 K (1100 °C).

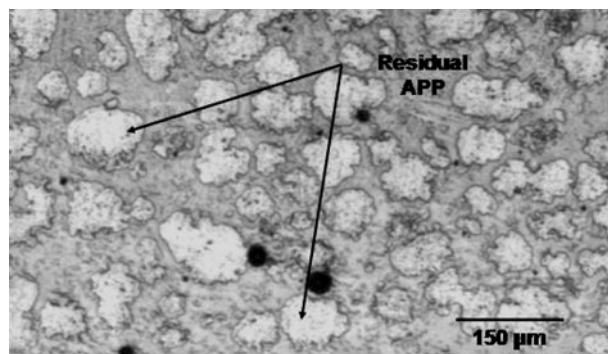


Fig. 11—Microstructure of Type 2 powder mixture with partially melted coarse APPs with  $R_{FA}$  of 7:3 at 1373 K (1100 °C).

SC substrates material due to incomplete APP melting. Incomplete melting occurs when the total amount of solute-transport into the APPs is sufficient to complement the extent of solvent addition to the liquid, through the melting of the powder particles, to dilute the liquid composition to the equilibrium liquidus value. Otherwise, complete melting occurs.

At a constant initial APPs size, the extent of melting is influenced by a combination of interdependent salient process variables that include (i)  $R_{FA}$ , (ii) bonding temperature, and (iii) initial concentration of MPD solute in the filler alloy powder ( $C_f$ ). As shown in Figure 12, for a given combination of temperature and  $C_f$ , an increase in  $R_{FA}$  increases the extent of APP melting and complete melting occurs above a critical value,  $(R_{FA})_c$ . The  $(R_{FA})_c$  decreases with increases in both temperature and  $C_f$  (Figures 13 and 14). Therefore, for a given combination of filler alloy powder with a constant  $C_f$  and APP size, complete melting of APPs is possible through a proper selection of bonding temperature for a fixed value of  $R_{FA}$  and vice versa. The

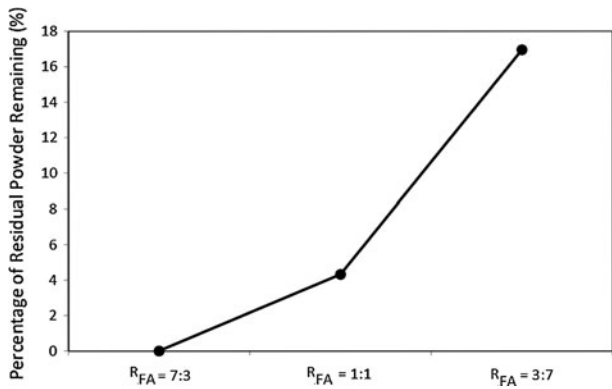


Fig. 12—Numerical simulation of percentage of residual APPs after 1 h holding time.

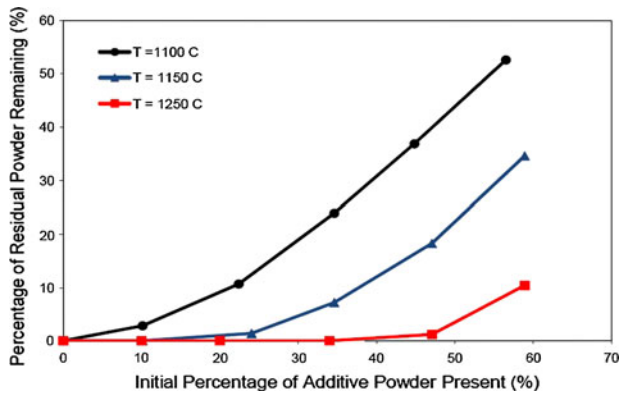


Fig. 13—Numerical simulation of the effect of temperature on the residual APPs.

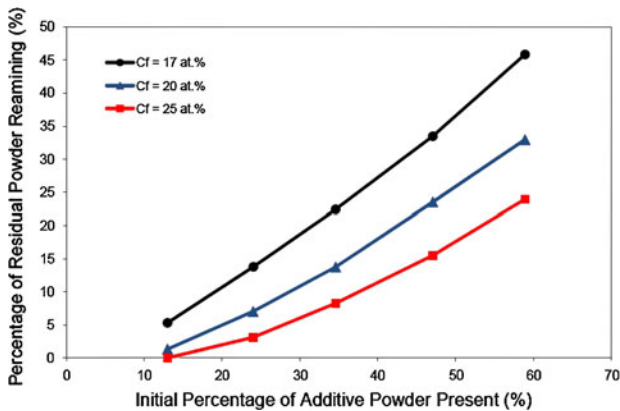
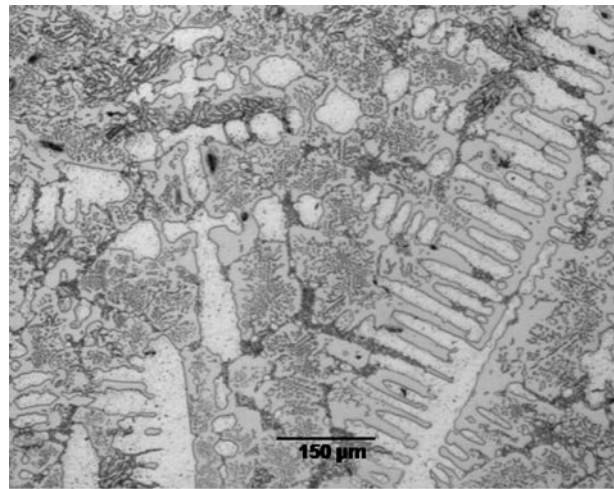
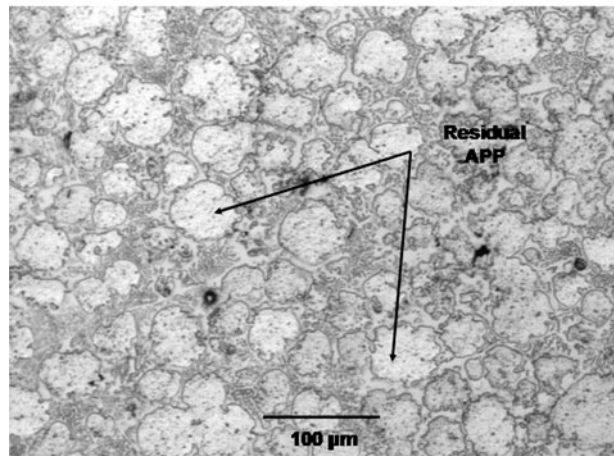


Fig. 14—Numerical simulation of the effect of initial concentration of MPD solute in the liquid,  $C_F$ , on the residual APPs.

numerically predicted behavior was experimentally confirmed. An increase in temperature from 1373 K to 1423 K (1100 °C to 1150 °C), for a fixed  $R_{FA}$  value of 7:3 resulted in the complete melting of coarse sized APPs (Figure 15a), which exhibited incomplete APP melting at 1373 K (1100 °C). Also, in agreement with the trend predicted by the numerical model, at a temperature of



(a)



(b)

Fig. 15—(a) Microstructure of powder mixture with completely melted coarse APPs with  $R_{FA}$  of 7:3 at 1423 K (1150 °C). (b) Microstructure of powder mixture with incompletely melted coarse APPs with  $R_{FA}$  of 1:1 at 1423 K (1150 °C).

1423 K (1150 °C), an increase in the  $R_{FA}$  from 7:3 to 1:1 produced incomplete melting of coarse sized APPs (Figure 15b).

The powder mixture that contained fine sized APPs with an  $R_{FA}$  of 7:3, which melts completely at 1423 K (1150 °C), was used as the interlayer material to produce a TLP joint between SC IN 738 substrate materials. Examination by scanning electron microscopy did not reveal any indication of stray-grains formation within the joint. Electron backscatter diffraction based crystallographic orientation imaging microscopy (OIM) was used to evaluate the crystallographic orientation relationship between the joint and the SC IN 738 substrate, to verify the preclusion of stray-grains within the joint. Randomly chosen points; 1, 2, 5, and 6 in the SC substrates, and points 3 and 4 in the joint region (Figure 16) were used in the OIM analysis. Stereographic inverse pole figures along three orientations; the plane of the joint (XO), the surface of the specimen (ZO) and the plane perpendicular to the joint and the specimen surface (YO), are shown in Figure 17. The

analysis showed that for all directions, XO, YO and ZO, the six points are projected at nearly the same location within the stereographic inverse pole figures. In addition, the {100}, {110} and {111} stereographic pole figures that include all of the analyzed six points are shown in Figure 18, which confirm the formation of a TLP joint that has matching crystallographic orientation with the substrate SC material. Therefore, even though the use of a powder mixture that contains APPs has been generally considered unsuitable for joining SC

materials, the understanding provided by the numerical analysis performed in this study coupled with experimental verification show that APPs can be effectively used for SC materials without the formation of stray-grains.

### C. Influence of APP Melting on Persistent Decrease in Isothermal Solidification Rate

A fundamental assumption in analytical TLP bonding models is that the diffusion-controlled displacement ( $J$ ) of liquid-solid interfaces during the isothermal solidification stage of the joining process follows a parabolic relationship with holding time,  $t$ , which is given by Reference 9:

$$J = 2\phi(t^{1/2}) \quad [21]$$

The extent of isothermal solidification during joining is influenced by an invariant parameter,  $\phi$ . It is implied in the analytical TLP bonding models that  $\phi$  is constant throughout the entire bonding process. Nevertheless, it has been found that although  $\phi$  can be constant while the solute concentration gradient within the base-material,  $\partial C/\partial x$ , decreases for a certain period of time, this may, however, cease to hold when the  $\partial C/\partial x$  decreases below a critical value  $(\partial C/\partial x)_c$ .<sup>[32]</sup> Reduction of  $\partial C/\partial x$  below  $(\partial C/\partial x)_c$  due to continual diffusion of the solute from the interlayer liquid into the substrate material will result in a persistent decrease in  $\phi$ .<sup>[32]</sup> The parameter  $\phi$  decreases with increase in the bonding temperature in systems where

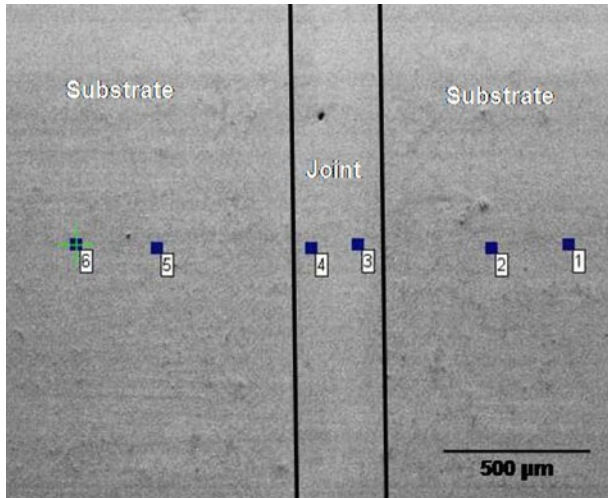


Fig. 16—TLP joint in SC IN 738 produced using powder mixture that contained completely melted APPs at 1423 K (1150 °C).

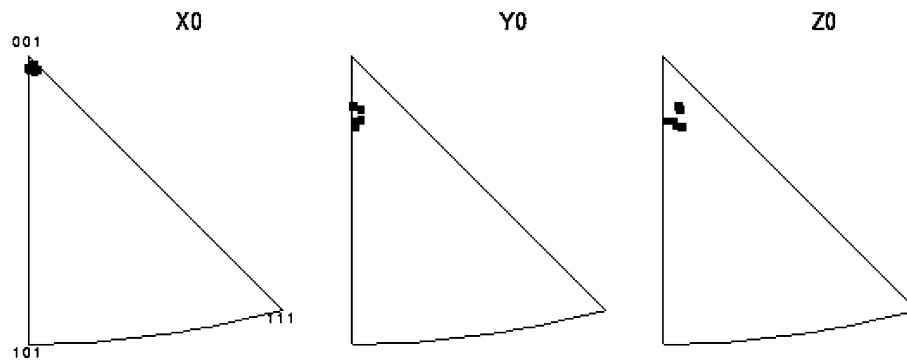


Fig. 17—Stereographic inverse pole figures showing the analyzed data points for the locations shown in Fig. 16.

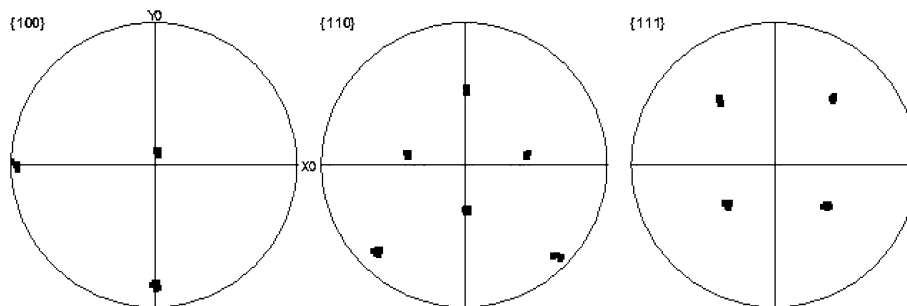


Fig. 18—{100}, {110} and {111} stereographic pole figures of the analyzed locations shown in Fig. 16.

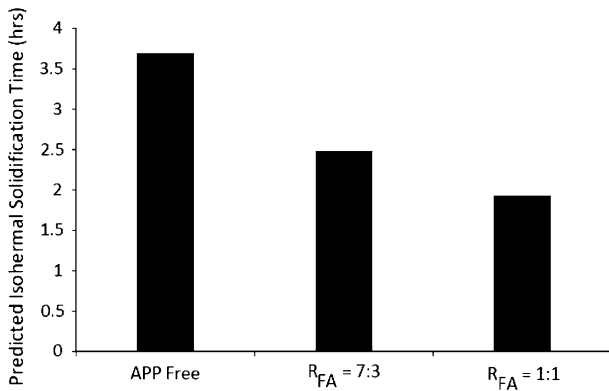


Fig. 19—Numerical simulation predicted isothermal solidification completion time at 1453 K (1180 °C).

the solubility of the MPD solute in the substrate decreases with increase in temperature, such as, in nickel-boron system. This can result in a situation where an increase in temperature will cause the time,  $t_f$ , required for the completion of isothermal solidification, to increase, notwithstanding the concomitantly increased solute diffusion coefficients at higher temperatures. This has been experimentally observed in Ni-base superalloys<sup>[33,34]</sup> and constitutes a major cause of increase in the processing time  $t_f$  during TLP bonding.

Accordingly, a possible approach to reducing  $t_f$  during TLP bonding is to limit the persistent decrease in  $\phi$  which occurs when  $\partial C/\partial x$  decreases below  $(\partial C/\partial x)_c$ . This can be achieved by reducing the amount of MPD solute required to diffuse into the base-material to produce complete isothermal solidification. The use of APPs, in a gap of a given size, effectively reduces the amount of MPD solute that is required to diffuse into the substrate material to achieve complete isothermal solidification. Therefore, complete melting of APPs, which is necessary to avoid stray-grains formation in SC materials, can limit the persistent decrease in the parameter  $\phi$ , and thus, reduce the  $t_f$  during TLP bonding of SC materials. This is supported by the numerical simulation results (Figure 19), which show that, for Ni-B system with initial gap size of 80  $\mu\text{m}$ , that complete APPs melting can produce a significant reduction in  $t_f$ . Experimental verification showed that the time  $t_f$  required to produce TLP joint free of stray-grains in SC IN 738 superalloy is reduced from 52 hours with the use of a 100 pct Microbraz 150 filler alloy powder to 26 hours with the use of an interlayer powder mixture that contains APPs with an  $R_{FA}$  of 7:3, for an initial gap size of 200  $\mu\text{m}$  at 1423 K (1150 °C). Therefore, proper analysis of APPs melting mechanisms enabled by the new numerical model developed in this work show that not only is the use of APPs suitable for SC materials, which is in contrast to previous conceptions, but its use can significantly reduce the processing time during the joining of SC materials. Moreover, the innovative approach used to develop the present hybrid model can aid the numerical simulation analysis of other propagating interphase boundaries that involve either the splitting or merging of migrating interfaces, which are generally difficult to be exclusively modeled by the classical finite element method.

#### IV. SUMMARY AND CONCLUSIONS

1. A robust numerical model that simultaneously captures solid-state solute diffusion within randomly distributed multiple APPs and their melting, which cannot be done by standard analytical models, has been developed by an interface-enriched extended finite element-level set method to enable the proper understanding of APP melting behavior during TLP bonding.
2. At variance with analytical models, numerical calculations by the new model show that solute-transport into APPs during the equilibration of the liquid composition is a crucial factor that influences the extent of APPs melting and this occurs through the kinetics of solid-state solute diffusion within the powder particles.
3. Accordingly, in contrast to what has been commonly assumed in the literature, the model predicts that complete melting of the APPs can occur during the equilibration stage of TLP bonding, depending on the combination of interdependent materials and process variables. These include APPs size, temperature, ratio of filler alloy powder particles to APP, ( $R_{FA}$ ), and initial concentration of MPD solute in the filler alloy powder ( $C_F$ ).
4. The understanding provided by the numerical analysis has resulted in the use of a powder mixture that consists of APPs to produce single crystal TLP joints that have matching crystallographic orientations with SC substrates, which has been previously considered unfeasible.
5. Moreover, the interlayer liquid produced by complete melting of the APPs limits persistent decreases in the  $\phi$ , and thus, reduces the time  $t_f$  that is required to produce joint that is free of stray-grains during TLP bonding of SC materials.

#### ACKNOWLEDGMENT

The authors gratefully acknowledge financial support by NSERC of Canada.

#### REFERENCES

1. S.D. Duvall and W.A. Owczarski: *Weld. J.*, 1967, vol. 46 (9), pp. 423–32.
2. O.A. Ojo and M.C. Chaturvedi: *Metall. Mater. Trans. A*, 2007, vol. 38A, pp. 356–69.
3. D.S. Duvall, W.A. Owczarski, and D.F. Paulonis: *Weld. J.*, 1974, vol. 53 (4), pp. 203–14.
4. A.A. Shirzadi and E.R. Wallach: *Acta Mater.*, 1999, vol. 47 (13), pp. 3551–60.
5. K. Tokoro, N. Wikstrom, O.A. Ojo, and M.C. Chaturvedi: *Mater. Sci. Eng. A*, 2008, vol. 477, pp. 311–18.
6. B. Dutta and M. Rettenmayr: *Metall. Mater. Trans. A*, 2000, vol. 31A, pp. 2713–20.
7. E. Gamsjager, J. Svoboda, F.D. Fischer, and M. Rettenmayr: *Acta Mater.*, 2007, vol. 55, pp. 2599–2607.
8. M. Buchmann and M. Rettenmayr: *J. Cryst. Growth*, 2008, vol. 310, pp. 4623–27.
9. Y. Zhou: *J. Mater. Sci. Lett.*, 2001, vol. 20, pp. 841–44.

10. Y. Zhou and T. North: *Model. Simul. Mater. Sci. Eng.*, 1993, vol. 1, pp. 505–16.
11. T.C. Illingworth and I.O. Golosnoy: *J. Comput. Phys.*, 2005, vol. 209, pp. 207–25.
12. J.F. Li, P.A. Agyakwa, and C.M. Johnson: *J. Mater. Sci.*, 2010, vol. 45, pp. 2340–50.
13. J.M. Melenk and I. Babuska: *Comput. Methods Appl. Mech. Eng.*, 1996, vol. 39, pp. 289–314.
14. D. Chopp and J. Dolbow: *Int. J. Numer. Methods Eng.*, 2002, vol. 54, pp. 1209–33.
15. N. Sukumar, D.L. Chopp, N. Moes, and T. Belytschko: *Comput. Methods Appl. Mech. Eng.*, 2001, vol. 190, pp. 6183–6200.
16. J. Chessa, H. Wang, and T. Belytschko: *Int. J. Numer. Methods Eng.*, 2003, vol. 57, pp. 1015–38.
17. R. Gracie, H. Wang, and T. Belytschko: *Int. J. Numer. Methods Eng.*, 2008, vol. 74 (11), pp. 1645–69.
18. T.P. Fries: *Int. J. Numer. Methods Eng.*, 2008, vol. 75, pp. 503–32.
19. T. Belytschko, W.K. Liu, and B. Moran: *Nonlinear Finite Elements for Continua and Structures*, John Wiley & Sons, New York, 2003, ISBN:0-471-98774-3.
20. H. Ji and J.E. Dolbow: *Int. J. Numer. Methods Eng.*, 2004, vol. 61, pp. 2508–35.
21. R. Duddu, D. Chopp, P. Voorhees, and B. Moran: *J. Comput. Phys.*, 2010, vol. 230, pp. 1249–64.
22. N. Moes, M. Cloirec, P. Cartraud, and J.F. Remacle: *Comput. Methods Appl. Mech. Eng.*, 2003, vol. 192, pp. 3163–77.
23. C.A. Soghrati, A.M. Aragón, A.M. Duarte, and P.H. Geubelle: *Int. J. Numer. Methods Eng.*, 2012, vol. 89 (8), pp. 991–1008.
24. N. Sukumar and J. Prevost: *Int. J. Solids Struct.*, 2003, vol. 40, pp. 7513–37.
25. S. Osher and J. Sethian: *J. Comput. Phys.*, 1988, vol. 79 (1), pp. 12–49.
26. S. Osher and R. Fedkiw: *Level Set Methods and Dynamic Implicit Surfaces*, Springer, New York, 2003, ISBN: 0-387-95482-1.
27. A. Ghoneim and O.A. Ojo: *Comput. Mater. Sci.*, 2011, vol. 50, pp. 1102–1113.
28. A. Ghoneim and O.A. Ojo: *Metall. Mater. Trans. A*, 2012, vol. 43A (3), pp. 900–11.
29. P.K. Liao and K.E. Spear: *Bull. Alloy Phase Diagr.*, 1986, vol. 7 (3), p. 550.
30. Y. Zhou, W.F. Gale, and T.H. North: *Int. Mater. Rev.*, 1995, vol. 40, pp. 181–196.
31. O.A. Idowu, O.A. Ojo, and M.C. Chaturvedi: *Metall. Mater. Trans. A*, 2006, vol. 37A, pp. 2787–96.
32. M.M. Abdelfattah and O.A. Ojo: *Metall. Mater. Trans. A*, 2009, vol. 40A, pp. 377–85.
33. Y. Xinjian, B.K. Myung, and Y.K. Chung: *Metall. Mater. Trans. A*, 2011, vol. 42A, pp. 1310–24.
34. M.K. Dinkel, P. Heinz, F. Pyczak, A. Volek, M. Ott, E. Affeldt, A. Vossberg, M. Goken, and R.F. Singer: *11th International Symposium on Superalloys*, 2008, pp. 211–20.